OPEN ACCESS

Ultrafast IR spectroscopic study of coherent phonons and dynamic spin–lattice coupling in multiferroic $LuMnO_3$

New Journal of Physics
The open-access journal for physics

Ultrafast IR spectroscopic study of coherent phonons and dynamic spin–lattice coupling in multiferroic $LuMnO_3$

Kyeong-Jin Jang[1], Jongseok Lim[1], Jaewook Ahn[1,5], Ji-Hee Kim[2], Ki-Ju Yee[2], Jai Seok Ahn[3,5] and Sang-Wook Cheong[4]

[1] Department of Physics, Korea Advanced Institute of Science and Technology, Daejeon 305-701, Korea
[2] Department of Physics, Chungnam National University, Daejeon 305-764, Korea
[3] Department of Physics and RCDAMP, Pusan National University, Pusan 609-735, Korea
[4] Rutgers Center for Emergent Materials and Department of Physics and Astronomy, Rutgers University, Piscataway, NJ 08854, USA
E-mail: jwahn@kaist.ac.kr and jaisahn@pusan.ac.kr

New Journal of Physics **12** (2010) 023017 (10pp)
Received 12 October 2009
Published 12 February 2010
Online at http://www.njp.org/
doi:10.1088/1367-2630/12/2/023017

Abstract. The concurrent existence of ferroelectricity and magnetism within a single crystalline system characterizes the multiferroic materials discovered in recent years. To understand and develop the multiferroic phenomenon, we need to investigate the unusual coupling between spin and lattice degrees of freedom. Spins in multiferroics are expected to be elastically coupled to phonons. Therefore, the time-dependent study can be a crucial factor in understanding the coupled dynamics. Here, we report the observations of strong dynamic spin–lattice coupling in multiferroic $LuMnO_3$. A coherent optical phonon of 3.6 THz and its temperature dependence is measured for the first time from our femtosecond IR pump and probe spectroscopy. Also, we observed a coherent acoustic phonon of 47 GHz similar to a previous report (Lim *et al* 2003 *Appl. Phys. Lett.* **83** 4800). Temperature-dependent measurements show that both optical and acoustic phonons become significantly underdamped as temperature

[5] Author to whom any correspondence should be addressed.

decreases to T_N, and they disappear below T_N. These observations reveal that phonons are coupled to spins by magneto-elastic coupling, and the disappearance of phonon modes at T_N is consistent with the isostructural coupling scheme suggested by Lee *et al* (2008 *Nature* **451** 805).

Contents

1. Introduction

Magnetism and ferroelectricity coexist in materials called multiferroics, resulting in a strong interplay between magnetic and dielectric properties. The coupling between dielectric and magnetic properties provides possibilities of controlling magnetic properties using electric fields and controlling dielectric properties using magnetic fields. As magnetism and electricity are important in developing material-based technologies, the research of multiferroic materials and their fundamental properties has become unprecedentedly competitive in recent years [1, 2].

Multiferroic materials are found in a class of materials known as *frustrated magnets*, for example the perovskites $RMnO_3$, RMn_2O_5, delafossite $CuFeO_2$, spinel $CoCr_2O_4$ and hexagonal ferrites [3]–[8]. Interestingly, the origin of the strong coupling between the dielectric and magnetic properties is not the magneto-electric coupling, but the magnetically induced ferroelectricity from complex spin structure [9]–[12]. In general, magneto-elastic coupling plays an important role in a magnetically complex system that contains weak or frustrated magnetic interactions. For example, in an antiferromagnetic spin-Peierls system such as $CuGeO_3$, spins couple to phonons elastically such that the translational symmetry is also spontaneously broken [13]. In a superconducting iron-pnictide system, the spin density wave couples to a structural distortion; therefore, superconductivity is recovered when the structural distortion is suppressed [14]. For a multiferroic system with geometrically frustrated magnets, spin fluctuations can cause unusual dynamic effects due to strong spin–lattice coupling. Therefore, especially in the vicinity of the magnetic phase transition, optical phonon generation and its time-dependent study can be used as a direct tool to study coupled dynamics between spin and lattice. As for the multiferroic properties, many studies have been conducted on crystallographies, optical properties and magnetic structural changes [15]–[17], but the interrelations between spin and lattice are not yet fully understood. Temperature-dependent studies have provided a better understanding of magneto-dielectric coupling by the measurements of crystal structures and dielectric constants [18]–[21]. Most importantly,

spin–lattice coupling has been observed in optical property, thermal conductivity and neutron diffraction [22]–[24].

In this paper, we have performed femtosecond time-resolved pump–probe reflection measurements of $LuMnO_3$ to investigate the dynamics of optically induced lattice vibrations near the antiferromagnetic phase transition. $LuMnO_3$ has a ferroelectric phase transition at high temperature ($\sim$900 K) and an antiferromagnetic phase transition at $T_N \sim$90 K. In a recent transport study of $LuMnO_3$, the dielectric constant changes anomalously as spin ordering appears below T_N [18]. A time-dependent study is useful to complement conventional optical methods for a better understanding of coupled dynamics. For these reasons, time-resolved optical spectroscopy was used to investigate the non-equilibrium states of a coupled system and it was useful to understand the physical properties of manganese oxide materials; see for example [25].

2. Experimental procedure

The experiment was carried out in a fast-scanning pump and probe spectroscopy setup. The lattice vibration of the sample was induced by an intense 20-fs-short pump pulse from a cavity-dumped Ti:sapphire laser oscillator, and then the optical reflectance was measured by a weak probe pulse as a function of time delay between the pump and probe pulses. The laser operated at a center wavelength of 790 nm ($\sim$1.57 eV) and at a repetition rate of 400 kHz. For a time delay between the pump and probe, a raster scanning shaker (APE Scan Delay) was used in the path of the pump pulse. The focused laser spots at the sample were $\sim$80 and $\sim$30 μm for the pump and probe pulses, respectively. Flux-grown $LuMnO_3$ single crystals were used. The sample was cleaved as platelets with a thickness of $\sim$100 μm. The polarization of the normally incident pump beam is independent of the orientation of the c-cut crystal and was kept perpendicular to the probe beam to minimize coherent artifacts and also scattered pump noise. The pump laser fluence was kept below 300 μJ cm^{-2} to minimize local heating of the sample. Our measurement setup operates at a higher repetition rate (400 times) and with a lower single pulse power (a few hundred times lower) than the amplifier-based setup used in [26]. The low power operation at a high repetition rate has been proven in our experiment, crucial for the low-temperature measurements. The spectrum of the pump laser was chosen to maintain the optical excitation for $LuMnO_3$ to be efficient and mildly varied over the measurement temperature range [22]. The temperature of the sample was varied from 5 to 300 K in a cryostat (JANIS ST-500) filled with liquid He.

3. Results and discussion

Figure 1 represents time-dependent changes of the optically induced lattice vibrations of $LuMnO_3$ measured as optical reflectance changes $\Delta R/R$ at various temperatures. Photo-induced reflectance change $\Delta R/R$ was measured as a function of time delay (t). Figure 1(a) represents the initial data ($t < 11$ ps) measured with high time resolution (time delay interval, $\Delta t = 1$ fs). Figure 1(b) shows the data of the entire range ($t < 110$ ps) measured with low resolution ($\Delta t = 10$ fs). In addition to the typical relaxation behavior, two types of coherent oscillations are observed: the 'fast' oscillation in figure 1(a) and the 'slow' oscillation in figure 1(b).

We applied Fourier transform (FT) analysis to obtain information in the frequency domain of the coherent oscillations. The FT results ($\Delta R(\omega)/R$) of the high- and low-frequency parts

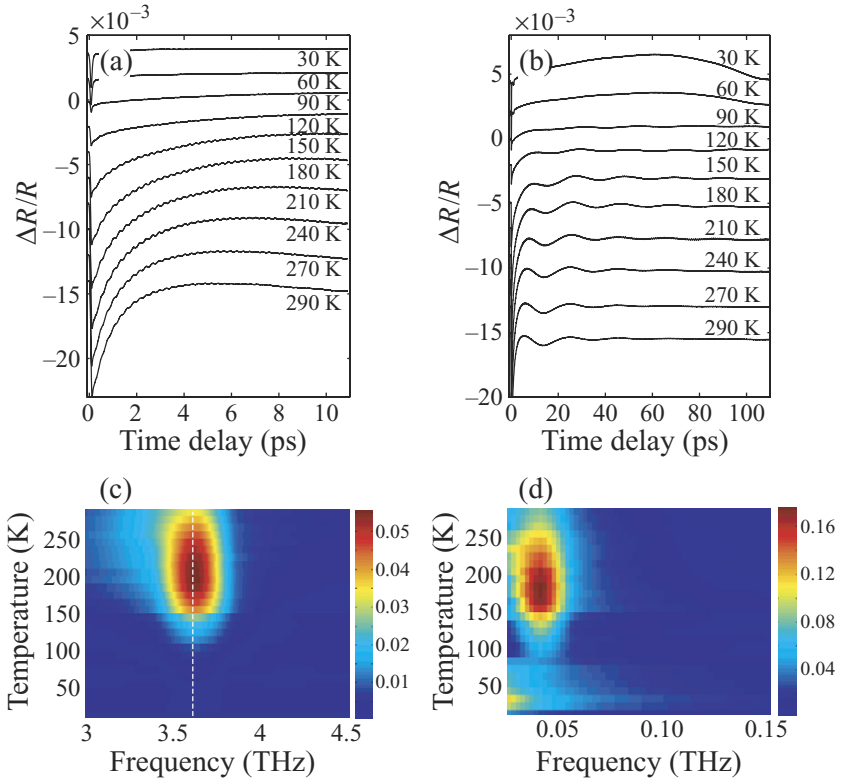

Figure 1. Photo-induced reflectance change $\Delta R(t)/R$ plotted as a function of time delay (t) for various temperatures: (a) time delay interval $\Delta t = 1$ fs and (b) $\Delta t = 10$ fs. Fourier-transformed amplitudes of a coherent optical phonon in (c) and a coherent acoustic phonon in (d). In (c), a dashed line represents optical phonon frequency from [22]. The reflectivity data in (a) and (b) are shifted along the vertical axis for clarity.

are separately obtained from $\Delta R(t)/R$ in figures 1(a) and (b), respectively. The FT results are displayed in figures 1(c) and (d) as 2D intensity plots as functions of frequency and temperature. The frequency of the 'fast' oscillation is found around ~ 3.6 THz. The measured frequency is similar to the lowest optical phonon mode (3.57 THz at room temperature) previously reported by Souchkov *et al* [22] for the $\vec{E} \parallel \vec{c}$ polarization. Therefore, the 'fast' oscillation can be assigned as an optical phonon mode. The frequency of the 'slow' oscillation is the strongest for ∼47 GHz at $T = 180$ K. Our result is in good agreement with Lim *et al*'s [26] report: they also found a coherent mode at ∼46 GHz (at $T = 180$ K) and assigned it as an acoustic phonon mode. However, the temperature dependence significantly differs from ours, especially near and below T_N. The FT amplitudes of optical and acoustic modes are plotted in figure 2(a). The amplitudes are obtained from the characteristic frequencies, i.e. 3.6 THz and 47 GHz. Both oscillations have a similar temperature dependence, which gradually disappear as the sample temperature approaches T_N from above. A similar disappearance of oscillation is found at the structural transitions in $SrTiO_3$, VO_2, $Pb_{1-x}Ge_xTe$ and $La_{0.42}Ca_{0.58}MnO_3$ [27]–[30]. To the best of our knowledge, this is the first observation indicating the coupling of coherent phonons with the antiferromagnetic ordering transition, i.e. through magneto-elastic coupling.

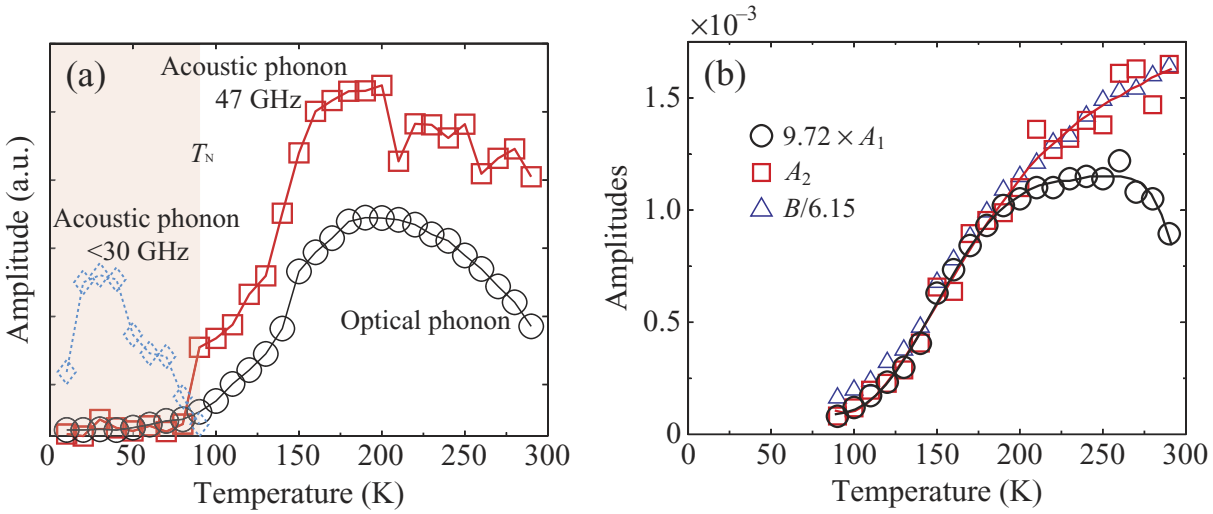

Figure 2. (a) Temperature dependence of the phonon amplitudes obtained by Fourier analysis. Below T_N, another smaller frequency appears in dashed diamonds. (b) Amplitudes obtained by model analysis using equation (1). The oscillation amplitude of the acoustic phonon (A_2) is plotted in squares and the optical modes in circles ($9.72 \times A_1$). The amplitude of the electronic relaxation ($B/6.15$) is shown with triangles. Curves are drawn after scaling. The lines are guides to the eye.

Pump–probe measurement probes Raman modes basically and, therefore, it is sensitive to the group symmetry change. Therefore, the disappearance of phonon modes at T_N can be related to the magneto-elastic coupling scheme of hexagonal manganites near T_N, suggested by the recent neutron study [20], the so-called giant magneto-elastic coupling in the isostructural transition in hexagonal manganites. In addition, another strange low-frequency overdamped component ($f < 30$ GHz) develops below T_N.

In order to elucidate the temporal decay behavior of the reflectance change precisely, we introduce an empirical model. The model consists of two oscillatory decays and a simple exponential decay:

$$\frac{\Delta R(t)}{R} = C + Be^{-\beta t} + \sum_{i=1,2} A_i e^{-\gamma_i t} \cos(\omega_i t + \phi_i), \tag{1}$$

where $\omega_{1,2}$ and $\gamma_{1,2}$ are the angular frequencies and damping constants of the coherent oscillations, and β is the non-oscillatory relaxation rate. Also, $A_{1,2}$, B and C are proportional amplitudes. With this model, we could successfully fit the reflectance change and could extract parameters such as amplitudes, frequencies, dephasing time constants, etc. The amplitude curves obtained with the model are plotted in figure 2(b), and they are similar to the results obtained with the FT method in figure 2(a). In figure 2(b) scaled results are presented. Interestingly, the amplitudes B and A_2 fall on a single curve, indicating a scaling relationship between them. Also, the amplitude A_1 scales with the other two amplitudes below $\sim$180 K. This scaling behavior suggests that there is strong coupling among the three objects, i.e. their populations (after excitation) are proportional to each other in the temperature axis.

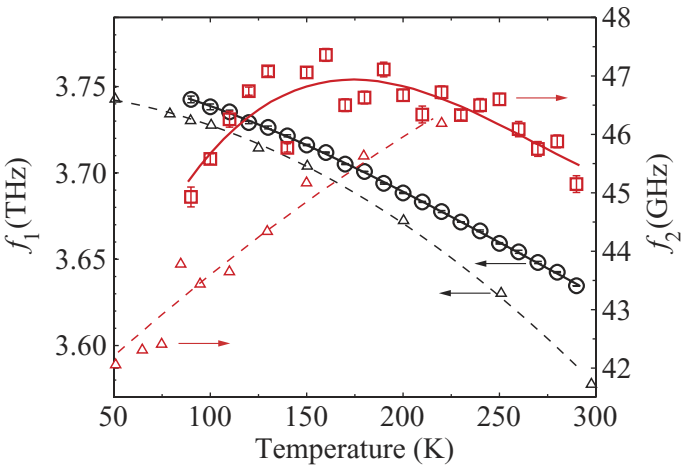

Figure 3. Temperature dependence of the mode frequencies f_1 ($=\omega_1/2\pi$) ('fast' mode, with black circles) and f_2 ($=\omega_2/2\pi$) ('slow' mode, with red squares). The reported optic phonon frequency from [22] is plotted with black triangles. The reported acoustic phonon frequency from [26] is plotted with red triangles: note that 400 nm pumping was used in their case. The lines are guides to the eye.

3.1. Optical coherent phonons

Furthermore, the temperature dependence of the frequency ($f_1 = \omega_1/2\pi$) can be analyzed using the model. The 'fast' mode shows hardening behavior as temperature is lowered from room temperature. The frequency is upshifted by less than 3% as the temperature decreases down to 90 K, as shown in figure 3. Such behavior is very close to Souchkov *et al*'s [22] report for an optical phonon ~3.57 THz, as compared in figure 3. The 'fast' oscillatory behavior of $\Delta R/R$ formulated in equation (1) is consistent with a characteristic behavior of reflectance change in the displacive excitation of coherent phonons (DECP) mechanism [31], which is a good candidate for the generation of coherent optical phonons in $LuMnO_3$. In DECP, the oscillatory changes of reflectance are caused by the change of electronic energy distribution due to an IR absorption occurring at the excitation energy. For hexagonal manganites, the electronic transition from ${}^5\Gamma_1(t_2^3e^1)$ to ${}^5\Gamma_5(t_2^2e^2)$, the on-site Mn d–d transition, occurs by a 1.6 eV pump pulse and the optical phonon accompanies the electronic excitation through an electron–phonon interaction [32, 33]. After a short pump–pulse excitation, the excited electron density goes to quasi-equilibrium much faster than the response of the nuclei. The excited electron density relaxes $\propto e^{-\beta t}$. The electronic response affects nuclear motion through the electron–lattice coupling. For deformational electron–phonon coupling, only zero wave vector phonon modes are coherently excited [34]. The equation of motion of nuclear coordinate $Q(t)$ can be given as a driven damped oscillator type with source $F_{\text{ext}}(t) \sim e^{-\beta t}$:

$$\frac{\partial^2 Q}{\partial t^2} + 2\gamma_1 \frac{\partial Q}{\partial t} + \omega_0^2 Q(t) = F_{\text{ext}}(t), \tag{2}$$

where ω_0 and γ_1 are the angular frequency and the damping constant of the mode. The fractional change in reflectivity, $\Delta R(t)/R$, due to the short-pulse excitation can be approximated as

proportional to the nuclear response $Q(t)$ and the electronic response $e^{-\beta t}$ [31]:

$$\frac{\Delta R}{R} = B_0 e^{-\beta t} + A_0 \frac{\omega_0^2}{\omega_0^2 + \beta^2 - 2\gamma_1\beta}\left[e^{-\beta t} - e^{-\gamma_1 t}\left\{\cos(\omega_1 t) - \frac{\beta'}{\omega_1}\sin(\omega_1 t)\right\}\right]$$
$$= (B_0 + A_0')e^{-\beta t} - \frac{A_0'}{\sqrt{1+(\beta'/\omega_1)^2}} e^{-\gamma_1 t}\cos(\omega_1 t + \phi_1), \quad (3)$$

where $A_0' = A_0\omega_0^2/(\omega_0^2 + \beta^2 - 2\beta\gamma_1)$, $\phi_1 = \tan^{-1}(\beta'/\omega_1)$, $\omega_1 \equiv \sqrt{\omega_0^2 - \gamma_1^2}$ and $\beta' = \beta - \gamma_1$. A_0 and B_0 are amplitudes from induced nuclear displacement and from excited electron population, respectively. Also, β and γ_1 are decay constants from electronic origin and from nuclear motion, respectively. Therefore, the DECP mechanism predicts the following: (i) nuclear relaxation is ascribed to oscillatory decay and (ii) electronic relaxation is mostly from simple exponential decay. The parts of equation (3) are the same as the two terms shown in equation (1), with the following substitutions: $A_1 = A_0'/\sqrt{1+(\beta'/\omega_1)^2}$ and $B = B_0 + A_0'$.

3.2. Strain pulse propagation

The 'slow' oscillatory behavior is also consistent with the prediction of the typical propagating strained layer mechanism for acoustic phonon generation [35]. There is an interference between probe beams reflected off the surface and the strained layer propagating with the speed of sound v_s. Therefore, the reflected probe pulse shows oscillatory behavior with time delay t:

$$\frac{\Delta R}{R} \propto \cos\left(\frac{4\pi n_0 v_s}{\lambda} t + \phi_2\right), \quad (4)$$

where λ is the wavelength of the probe pulse and n_0 is the index of refraction without strain. The frequency of the oscillation is given as $\omega_2 = 4\pi n_0 v_s/\lambda$. Equation (4) shows the same temporal behavior as the slow oscillatory part of equation (1), assuming the dephasing of acoustic mode observed in our experiment. The 'slow' oscillation in figure 1(b) is analyzed with this mechanism and the temperature dependence of the mode frequency ($f_2 = \omega_2/2\pi$) is shown in figure 3. The 'slow' mode hardens as temperature is lowered to ~160 K, and this behavior is consistent with the temperature dependence of other optical phonons [22]. However, the 'slow' mode changes into weakly softening behavior below ~160 K down to 90 K. This temperature dependence is different from Lim *et al*'s [26] report with a 400 nm pumping laser, as compared in figure 3. Note that a 790 nm laser is used in our case, which is close to the resonant d–d transition condition of $LuMnO_3$ [32, 33]. The electronic level transition in the resonance is $d_{(x^2-y^2)',(xy)'} \rightarrow d_{(3z^2-r^2)'}$, and the occupied $d_{(3z^2-r^2)'}$ orbital is closely responsible for the short-range antiferromagnetic correlations above T_N, which have been observed in this geometrically frustrated magnetic system [18].

3.3. Dephasing and relaxation

The dephasing times of phonons, shown in figure 4, also indicate strong temperature dependences. They increase significantly as temperature decreases to T_N, i.e. the coherent phonons become underdamped. The phonon dephasing times ($\tau_{d,1}$ and $\tau_{d,2}$) and the electronic relaxation time ($1/\beta$) increase five times as temperature decreases from 290 to 90 K. The smaller

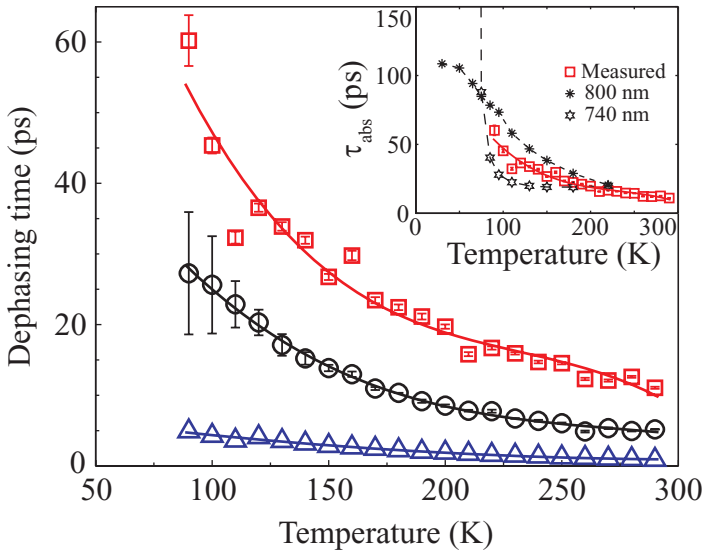

Figure 4. Temperature dependence of dephasing times: $\tau_{d,1}$ $(=1/\gamma_1)$ (optic phonon, with circles) and $\tau_{d,2}$ $(=1/\gamma_2)$ (acoustic phonon, with squares). The electronic relaxation time $(1/\beta)$ is also shown with triangles. In the inset, the temperature dependence dephasing time of the 47 GHz coherent acoustic phonon is shown (red squares). Asterisks and stars represent dominant absorption time constants, $\tau_{abs} = \lambda/4\pi v_s \kappa$, for 800 and 740 nm, respectively. Here the extinction coefficients, κ, are from [26]. The lines are guides to the eye.

values of the electronic relaxation time indicate that excited electrons relax faster than nuclei, as stated above in the DECP mechanism. Because the acoustic dephasing time is much longer than others, skin depth should also be considered. The skin depth is estimated as ~130 nm using the dielectric constant $\tilde{\epsilon} = 7 + 5.5\mathrm{i}$ at 790 nm. The propagating length of the strain pulse is much longer than the skin depth of the probe beam. Therefore, the absorption time constant, $\tau_{abs} = \lambda/4\pi v_s k$ [26], is dominant in the dephasing process. As temperature decreases, τ_{abs} increases, because k (for $\lambda = 790$ nm) decreases in $LuMnO_3$.

3.4. Spin–phonon coupling

Regarding the acoustic phonon, our observations are the following: (i) the acoustic phonon frequency in figure 3 has softening behavior below ~160 K and (ii) the phonon mode is not excited below T_N, as shown in figure 2. According to the thermal analysis by Sharma *et al* [23], the acoustic phonon can be strongly coupled to spin fluctuations above and below T_N. In the high-temperature phase near and above T_N, the interacting spins fluctuate energetically among the nearly degenerate ground state configurations originating from geometric frustration. Therefore, a generic spin coupling to phonons at the phase transition temperature can be a cause of the observed critical behavior of spin scattering [36]–[38].

For the optical phonon, the anomalous behavior in figure 2 suggests spin–phonon coupling that occurs in the magnetically ordered phase below T_N. $LuMnO_3$ has structural change across the ferroelectric phase transition temperature (~900 K) from the higher symmetry space group $P6_3/mmc$ to $P6_3cm$ [39]. However, there is no structural transition at T_N. From this point,

the anomalous behavior is not induced by pure structural phase transition. Similar anomalies observed in $SrRuO_3$ (ferromagnet) have been explained by ion motions that modulate spin exchange coupling [40]. The measured 3.6 THz mode includes displacement of Lu ions along the *c*-axis, and the anomalous change of this mode indicates spin–phonon coupling below T_N. Recently, an iso-structural transition was observed at T_N [20], i.e. each ion moves within the unit cell when Mn moments get ordered while the unit cell itself remains intact. This observation provides evidence for magneto-elastic coupling in the hexagonal manganites [41].

4. Conclusions

We measured the temperature dependence of coherent phonons of multiferroic $LuMnO_3$ using femtosecond pump–probe differential reflectance spectroscopy. The coherent oscillations of optic and acoustic modes were found to be above T_N, and these findings suggest the existence of strong spin–lattice coupling. The time dependence of coherent phonons was understood with DECP and propagating strain mechanisms. The electronic level transition, $d_{(x^2-y^2)',(xy)'} \rightarrow d_{(3z^2-r^2)'}$, is the driving source of the coherent modes near the resonance condition. The excited $d_{(3z^2-r^2)'}$ electron is responsible for the spin order in this geometrically frustrated magnetic system and it also couples to the phonon modes through the DECP mechanism. Therefore, our time-domain spectroscopic result supports Sharma *et al*'s [23] dynamic spin–phonon picture. The disappearance of phonon modes at T_N is consistent with the recent iso-structural transition picture suggested by Lee *et al* [20]. In summary, our observations for multiferroic $LuMnO_3$ show that (i) spin ordering couples to the excitation of both optic and acoustic phonons and (ii) spin fluctuation couples to the acoustic phonon.

Acknowledgments

This work was supported in part by the Basic Science Research Program through the National Research Foundation of Korea (NRF) funded by the Ministry of Education, Science and Technology (No. 2009-0090843) (KAIST) and in part by MOEHRD Grant KRF-2006-005-J02801 (PNU).

References

[1] Eerenstein W, Mathur N D and Scott J F 2006 *Nature* **442** 759
[2] Cheong S-W and Mostovoy M 2007 *Nat. Mater.* **6** 13
[3] Kimura T, Goto T, Shintani H, Ishizaka K, Arima T and Tokura Y 2003 *Nature* **426** 55
[4] Hur N, Park S, Sharma P A, Ahn J S, Guha S and Cheong S-W 2004 *Nature* **429** 392
[5] Smolenskif G A and Chupis I E 1982 *Sov. Phys.—Usp.* **25** 475
[6] Kimura T, Lashley J C and Ramirez A P 2006 *Phys. Rev.* B **73** 220401
[7] Yamasaki Y, Miyasaka S, Kaneko Y, He J-P, Arima T and Tokura Y 2006 *Phys. Rev. Lett.* **96** 207204
[8] Kimura T, Lawes G and Ramirez A P 2005 *Phys. Rev. Lett.* **94** 137201
[9] Lawes G *et al* 2005 *Phys. Rev. Lett.* **95** 087205
[10] Katsura H, Nagaosa N and Balatsky V 2005 *Phys. Rev. Lett.* **95** 057205
[11] Mostovoy M 2006 *Phys. Rev. Lett.* **96** 067601
[12] Sergienko I A and Dagotto E 2006 *Phys. Rev.* B **73** 094434

[13] Hirota K, Cox D E, Lorenzo J E, Shirane G, Tranquada J M, Hase M, Uchinokura K, Kojima H, Shibuya Y and Tanaka I 1994 *Phys. Rev. Lett.* **73** 736
[14] Chen G F, Li Z, Wu E, Li G, Hu W Z, Dong J, Zheng P, Luo J L and Wang N L 2008 *Phys. Rev. Lett.* **100** 247002
Yildirim T 2009 *Physica* C **469** 425
[15] Yakel H L, Koehler W C, Bertaut E F and Forrat E F 1963 *Acta Crystallogr.* **16** 957
[16] Iliev M N, Lee H-G, Popov V N, Abrashev M V, Hamed A, Meng R L and Chu C W 1997 *Phys. Rev.* B **56** 2488
[17] Munoz A, Alonso J A, Martinez-Lope M J, Casais M T, Martinez J L and Fernandez-Diaz M T 2000 *Phys. Rev.* B **62** 9498
[18] Katsufuji T *et al* 2002 *Phys. Rev.* B **66** 134434
Katsufuji T, Mori S, Masaki M, Moritomo Y, Yamamoto N and Takagi H 2001 *Phys. Rev.* B **64** 104419
[19] Van Aken B B and Palstra T T M 2004 *Phys. Rev.* B **69** 134113
[20] Lee S *et al* 2008 *Nature* **451** 805
[21] Tomuta D G, Ramarkrishnan S, Nieuwenhuys G J and Mydosh J A 2001 *J. Phys.: Condens. Matter* **13** 4543
[22] Souchkov A B, Simpson J R, Quijada M, Ishibashi H, Hur N, Ahn J S, Cheong S-W, Millis A J and Drew H D 2003 *Phys. Rev. Lett.* **91** 027203
[23] Sharma P A, Ahn J S, Hur N, Park S, Kim S B, Lee S, Park J-G, Guha S and Cheong S-W 2004 *Phys. Rev. Lett.* **93** 177202
[24] Lee S, Pirogov A, Han J H, Park J-G, Hoshikawa A and Kamiyama T 2005 *Phys. Rev.* B **71** 180413
[25] Averitt R D and Taylor A J 2002 *J. Phys.: Condens. Matter* **14** R1357
[26] Lim D, Averitt R D, Demsar J, Taylor A J, Hur N and Cheong S-W 2003 *Appl. Phys. Lett.* **83** 4800
[27] Lim D, Thorsmolle V K, Averitt R D, Jia Q X, Ahn K H, Graf M J, Trugman S A and Taylor A J 2005 *Phys. Rev.* B **71** 134403
[28] Kohmoto T, Tada K, Moriyasu T and Fukuda Y 2006 *Phys. Rev.* B **74** 064303
[29] Lu R, Hase M, Kitajima M, Nakashima S and Sugai S 2007 *Phys. Rev.* B **75** 012107
[30] Kim H-T, Lee Y W, Kim B J, Chae B G, Yun S J, Kang K Y, Han K J, Yee K J and Lim Y S 2006 *Phys. Rev. Lett.* **97** 266401
[31] Zeiger H J, Vidal J, Cheng T K, Ippen E P, Dresselhaus G and Dresselhaus M S 1992 *Phys. Rev.* B **45** 768
[32] Kimel A V, Pisarev R V, Bentivegna F and Rasing T 2001 *Phys. Rev.* B **64** 201103
[33] Degenhardt C, Fiebig M, Fröhlich D, Lottermoser T and Pisarev R V 2001 *Appl. Phys.* B **73** 139
[34] Kuznetsov A V and Stanton C J 1994 *Phys. Rev. Lett.* **73** 3243
[35] Liu R, Sanders G D, Stanton C J, Kim C S, Yahng J S, Jho Y D, Yee K J, Oh E and Kim D S 2005 *Phys. Rev.* B **72** 195335
[36] Kawasaki K 1963 *Prog. Theor. Phys.* **29** 801
Stern H 1965 *J. Phys. Chem. Solids* **26** 153
[37] Lewis F B and Saunders N H 1973 *J. Phys. Solid C State Phys.* **6** 2525
[38] Tsui Y K, Burns C A, Snyder J and Schiffer P 1999 *Phys. Rev. Lett.* **82** 3532
[39] Fukumura H, Matsui S, Harima H, Kisoda K, Takahashi T, Yoshimura T and Fujimura N 2007 *J. Phys.: Condes. Matter* **19** 365239
[40] Iliev M N, Litvinchuk A P, Lee H-G, Chen C L, Dazneti M L, Chu C W, Ivanov V G, Abrashev M V and Popov V N 1999 *Phys. Rev.* B **59** 364
[41] Fabrèges X, Petit S, Mirebeau I, Pailhès S, Pinsard L, Forget A, Fernandez-Diaz M T and Porcher F 2009 *Phys. Rev. Lett.* **103** 067204